Susceptibility-Based Imaging of Glioblastoma Microvascularity at 8 T: Correlation of MR Imaging and Postmortem Pathology

Gregory A. Christoforidis, Allahyar Kangarlu, Amir M. Abduljalil, Petra Schmalbrock, Abhik Chaudhry, Alan Yates and Donald W. Chakeres

AJNR Am J Neuroradiol 2004, 25 (5) 756-760
http://www.ajnr.org/content/25/5/756

AJNR Am J Neuroradiol 25:756–760, May 2004

Susceptibility-Based Imaging of Glioblastoma Microvascularity at 8 T: Correlation of MR Imaging and Postmortem Pathology

Gregory A. Christoforidis, Allahyar Kangarlu, Amir M. Abduljalil, Petra Schmalbrock, Abhik Chaudhry, Alan Yates, and Donald W. Chakeres

BACKGROUND AND PURPOSE: **Imaging methods are currently being optimized in an attempt to assess and monitor angiogenesis in vivo. The purpose of this investigation was to determine whether areas of apparently increased tumor vascularity, as identified on 8-T gradient-echo (GE) imaging of a known glioblastoma multiforme (GBM), corresponds to foci of increased microvascularity on histopathologic analysis.**

METHODS: **We performed postmortem in situ, high-resolution GE 8-T MR imaging of the brain in a 53-year-old woman with GBM. Ten histopathologic specimens in the region of the tumor bed were studied by using hematoxylin-eosin and reticulin stains. MR and histopathologic results were assessed and compared for microvascular size and density.**

RESULTS: **8-T GE images showed small, penetrating vessels in the gray matter and white matter. The images, however, were partly inhomogeneous as a result of local magnetic field inhomogeneities adjacent to the skull base and aerated paranasal sinus structures. 8-T MR images demonstrated serpiginous areas of signal intensity loss, which were thought to represent areas of increased microvascularity. Areas of lower microvascularity in the tumor bed corresponded to areas of lower vascularity on histopathologic sections with smaller vessel diameters. There was concurrence between vascular size predicted by histopathologic analysis and 8-T MR imaging in nine of nine biopsy samples. Vascular density agreed in seven of nine biopsy samples.**

CONCLUSION: **Our pilot data suggest that microvascularity in GBM can be identified by use of high-resolution, GE, 8-T MR imaging.**

The concept that tumor growth depends on angiogenesis has been refined over the past 3 decades (1, 2). Antiangiogenesis therapy is targeted toward the reduction of tumor vascularity. As a result, imaging methods are currently being optimized in an attempt to assess and monitor angiogenesis in vivo. Histopathologic methods to grade angiogenesis have been based on the number of vessels, on the degree of glomeruloid vascular structure formation, and on endothelial cytology (2). More recently, microvascular density (MVD) counting with panendothelial staining techniques has been used to quantify angiogenesis and has been found to act as an independent predictor (3–5). Imaging assessment of MVD in a tumor bed may indicate tumoral angiogenesis. However, MVD is not a direct measure of the functional status of tumor angiogenesis. Such a marker would have to more directly assess endothelial proliferative activity.

The purpose of this investigation was to determine whether areas of apparently increased tumor vascularity, as identified at 8-T gradient-echo (GE) imaging of a known glioblastoma multiforme (GBM), corresponds to foci of increased microvascularity on histopathologic analysis.

Methods

We compared in situ, postmortem 8-T MR images of a biopsy-proved GBM in a 53-year-old woman with the corresponding histopathologic sections. This patient had undergone biopsy and debulking of this neoplasm 3 months before her death and external beam irradiation 1 month after surgery. The patient eventually died after her neoplasm continued to progress. Consent for autopsy was obtained without restriction. Postmortem examination included high-resolution MR imaging at a field strength of 8 T by using a two-dimensional,

Received June 13, 2003; accepted after revision October 24.

From the Departments of Radiology (G.A.C., A.K., A.M.A., P.S., D.W.C.) and Pathology (A.C., A.Y.), the Ohio State University Medical Center, Columbus.

This study was supported by NCI grant 1R21CA/NS92846-01A1.

Address reprint requests to Gregory A. Christoforidis, Associate Professor Department of Radiology, the Ohio State University Medical Center, 627 Means Hall 1654 Upham Drive Columbus, OH 43221.

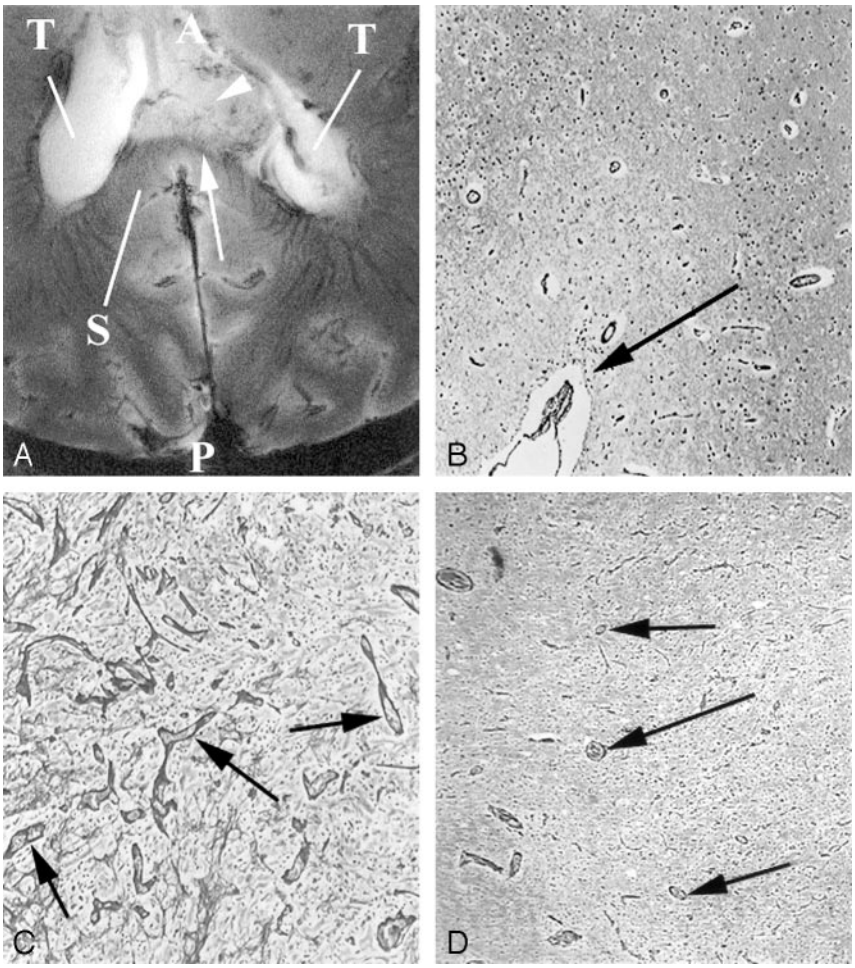

FIG 1. Images from the intact cadaver of a patient with known GBM.

A, Axial 8-T GE MR image (matrix = 1024 × 1024;TR/TE = 600/12; flip angle = 20°) in the patient with GBM at the level of the trigone of the lateral ventricles (*T*) and the level of the splenium (*S*) demonstrates an exophytic mass extending into the left lateral ventricle. *A* = anterior, *P* = posterior.

B–D, Reticulin-stained sections (original magnification ×100) correspond to an area of normal gray matter (*B*), the focus depicted by the *arrow* in *A* (*C*), and the focus depicted by the *arrowhead* in *A* (*D*). The *arrow* in *B* depicts the sulcus. Image in *C* shows an area of high vascular density and large vessels. Image in *D* corresponds to an area of vascularity and vessel size similar to that of the gray matter in the tumor bed. Vessels are depicted by *arrows* in *C* and *D*.

Fourier transformation GE sequence with flip angle of approximately 20°, a TR/TE of 500/10, a matrix of 1024 × 1024, a field of view (FOV) of 20 cm, a section thickness of 2 mm, and an acquisition time of 10 minutes. Radio-frequency (RF) spoiling and 250 microseconds of gradient spoiling along the section direction reduced residual transverse coherence. As such, the in-plane pixel size was 196 μm. The 8-T images were acquired on a commercial console (Bruker, Billerica, MA) by using a custom-built RF front end (6). A modified two-port, quadrature-drive, transverse electromagnetic (TEM) RF volume coil (7) was individually tuned on the patient's head. The head coil was placed inside the bore of the 8-T, 80-cm magnet (GE–Magnex Scientific, Abingdon, England).

Two neuroradiologists (G.A.C., D.W.C.) identified foci of enlarged microvasculature and foci of tortuous vascularity in the tumor bed on the 8-T images (Figs 1A and 2A). The size of the tumor vessels was compared with that of normal cortical-penetrating vessels. They were determined to be small if they were smaller than cortical penetrating vessels, medium if they were equal to cortical penetrating vessels, and large if they were larger than cortical-penetrating vessels in diameter.

Similarly, vessel density on 8-T images was estimated relative to cortical- and white matter–penetrating vessels and graded as high if the density was greater than that gray matter, medium if the density was between that of white matter and gray matter, and low if it was less than that of white matter. In addition, a method for measuring apparent vascular density in the tumor bed was adapted from that of Abramovitz et al (8–10). Regions of 5 mm were identified in the tumor bed and, the average signal intensity in this region was measured by using National Institutes of Health image software (version 1.62; National Institutes of Health, Bethesda, MD). In addition, the signal intensity of the entire tumor bed visible at 8-T MR imaging was measured. Angiogenic contrast (AC) was defined as the ratio of the average signal intensity from each region sampled (Sa) from the tumor bed to the average signal intensity from the entire tumor bed visible at MR imaging (So), as follows: So − AC = So/Sa. Apparent vascular density (ASD) was then defined as ASD = −ln(AC) (8–10). The values obtained were then used to assist in grading vascular density in the tumor bed.

Immediately after 8-T imaging, the patient's body was taken to autopsy, when the brain was removed without fixation and sectioned parallel to the plane of imaging. Specimens were then obtained from 10 regions in the brain corresponding to foci identified at 8-T MR imaging. Specimen locations were based on the corresponding topography identified on the basis of autopsy and imaging findings. Anatomic landmarks near the tumor, including the corpus callosum, the lateral ventricle, the medial atrial vein, the septum pallucidum, the vein of Galen, and the cortical sulci, were used to accurately match the location of the tissue sample to the corresponding location on the 8-T MR images. Furthermore, because the tumor protruded into the left lateral ventricle and invaded the septum pallucidum, the corresponding anatomy was readily identified by both imaging and autopsy. Sample locations were estimated on the image by interpolating the fraction of the distance between the closest anatomic landmarks and the sampling site at autopsy. For example, if a sampling site was located two-thirds the distance between the junction of the septum pallucidum with the lateral ventricle and the tumoral edge along the lateral ventricle, this site was also identified on the 8-T MR image. We made a similar calculation from other nearby anatomic sites, taking into account all three dimensions. Anatomic landmarks

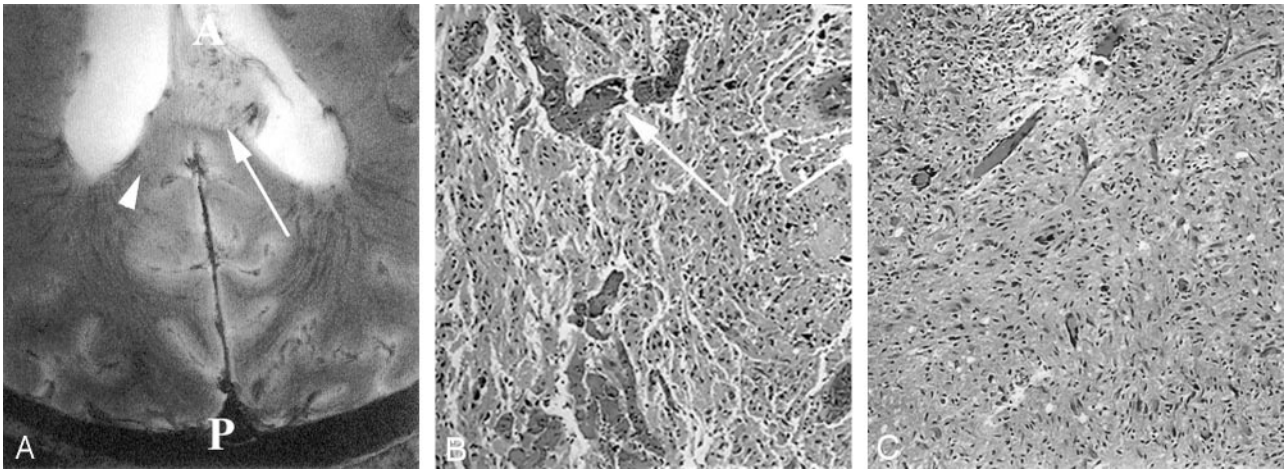

FIG 2. Additional images from the intact cadaver of a patient with known GBM.

A, Axial 8-T GE MR image (matrix = 1024 × 1024;TR/TE = 600/12; flip angle = 20°) in the patient with known GBM involving the splenium of the corpus callosum. This is 2 mm superior to the image in Figure 1A. Numerous small vessels are visible in the tumor bed. *A* = anterior, *P* = posterior.

B and *C*, Hematoxylin-eosin–stained sections (original magnification ×200) to the foci depicted by the *arrow* in *A* (*B*) and the arrowhead in *A* (*C*). *B*, Histologic specimen shows larger vessels (*arrow*) in dense concentration. Vessels in this region of exophytic tumor are also severely deformed in *A*, with loss of normal organization. Vessels can be seen crossing from the corpus callosum into the tumor. *C*, Image shows tumor infiltration with vascular density similar to white matter.

This table compares findings on 8T gradient echo MRI to histopathologic findings from corresponding foci within the patient's brain studied here. Comparisons include whether tumor was identified in each of the modalities (8T and histopathology), vessel size relative to normal brain tissues and vessel density relative to normal tissues

Identification of tumor		Vessel size		Vessel density	
8T	Pathology	8T vessel size	Histopathologic vessel size	8T vessel density	Histopathologic vessel density
No	Yes	small	small	low	low
Yes	Yes	large	large	high	high
Yes	Yes	small	small	low	medium
Yes	Yes	medium	medium	medium	medium
Yes	Yes	medium	medium	low	low
Yes	Yes	large	large	high	high
No	No	large	large	low	low
No	No	large	large	low	low
Yes	Yes	large	large	low	medium
Yes	Yes	necrosis	necrosis	necrosis	necrosis

were 15 mm from sampling sites at autopsy. The two neuroradiologists (G.A.C., D.W.C.) and two neuropathologists (A.Y., A.C.) agreed that the sampling sites corresponded to the imaging sites. Sampling included areas demonstrating high vascularity on 8-T imaging, areas of lower vascularity in the tumor bed on the images, and normal-appearing areas. (Table 1).

Tissue specimens were stained with hematoxylin-eosin to characterize the tumor in a standard fashion. Reticulin fiber stain was used to outline vascular walls and to analyze tumor vascularity. Specimens were also stained with Perl stain to determine whether iron deposition was present. The diameter of the microvascular structures and vascular density in each specimen was compared with that in normal cortex and normal white matter. Two experienced neuropathologists (A.Y., A.C.) graded these findings as high, medium, or low. Biopsy samples were also analyzed for the degree of tumor infiltration and the presence of necrosis and hemorrhage.

We compared semiquantitative assessments of microvascular size and density at 8-T MR imaging and histopathology. Reproducibility of the measures of microvascularity with either modality was not assessed because our sample was too small to make this type of analysis meaningful.

Results

8-T GE images could show small, penetrating vessels in the gray matter and white matter. The images, however, were partly inhomogeneous as a result of local magnetic field inhomogeneities adjacent to the skull base and aerated paranasal sinus structures and in part related to B1 RF coil inhomogeneities. The areas of interest were not significantly hampered by these artifacts, and visualization of the microvasculature in these regions was good.

The 8-T MR images demonstrated serpiginous areas of signal intensity loss, which were thought to represent areas of increased microvascularity (Fig 1). Areas of lower microvascularity in the tumor bed corresponded to areas of lower vascularity on histopathologic sections with smaller vessel diameters (Table). Foci of signal intensity loss surrounded areas of increased vascularity. Histopathologic analysis indicated that this was probably related to areas of

increased microvascularity. There was no histopathologic evidence on these stained specimens that this finding was related to hemosiderin deposition. Furthermore, no evidence of iron deposition was identified on the Perl stains.

Areas of brain with a normal MR imaging appearance that were adjacent to the tumor bed contained neoplastic cells (Fig 2). There was concurrence between vascular size predicted by histopathologic analysis and 8-T MR imaging in nine of nine biopsy samples. Vascular density agreed in seven of nine biopsy samples.

Discussion

The signal-to-noise ratio increases with field strength (11–18). Imaging at higher field strengths thus allows for imaging with a larger matrix, thinner sections, or faster acquisition times. On the other hand, magnetic susceptibility also increases with higher field strength and can result in signal-intensity loss and image distortion near the skull base and air spaces, as well as with paramagnetic substances, longer T1 times, or shorter T2 and T2* times (12, 19). Unlike spin-echo imaging that suppresses local field inhomogeneities, GE imaging with relatively longer TEs becomes highly sensitive to paramagnetic substances, such as deoxyhemoglobin (12, 18–20). Susceptibility effect by using GE imaging and high magnetic field strength increases the conspicuity of paramagnetic substances because of relative signal intensity loss. As a result, in vivo high-field-strength MR imaging at 8 T with a large matrix can show vasculature as small as 100 μm (20). Because this study was done after the patient's death, all vessels were expected to contain concentrations of deoxyhemoglobin higher than those in live patients. Therefore all vessels—arteries and veins—should be visualized with higher sensitivity on 8-T GE MR imaging, in contrast to similar examinations performed in vivo where the arterial tree (which contains little deoxyhemoglobin) is substantially less conspicuous than the deoxyhemoglobin-containing venous structures (11, 12). It is intuitive that any signal void due to flowing blood in blood vessels would not be possible post mortem. Vascular signal voids observed post mortem should result from hemoglobin in paramagnetic states. Susceptibility effects produced with GE imaging are increasingly visible (lower signal intensity) as TE increases; this leads to significant geometric distortion of images acquired near the skull base and air spaces (12, 19). Thus, even though susceptibility effect resulting from the use of longer TEs improves visualization of microvascular structures, it also results in greater geometric distortion. Images produced by using the parameters chosen for this study showed little distortion, with the exception of structures adjacent to the skull base.

In a study of 1440 malignant astrocytomas, Burger et al (21) found that, among histopathologic features such as cell density, nuclear atypia, mitotic activity, necrosis, and vascular proliferation, only vascular proliferation differentially predicted short- and long-term survival of patients with anaplastic astrocytomas. Currently, the identification of vascular proliferation in an astrocytoma places the tumor in World Health Organization classification IV. Typically, vascular proliferation is not uniform throughout a glial neoplasm. Because critical portions of a resected brain tumor are not always delivered with the specimen to a pathologist, critical markers of tumor grade may be overlooked, leading to potential undergrading of the tumor. As a result, in vivo imaging of features suggestive of a high grade in an astrocytoma (eg, increased vascularity) could play an important role in assigning tumor grade (21, 22).

The angioarchitecture and perfusion of a tumor is known to differ from that of normal brain: Vessels in the tumor bed are more tortuous, larger, and disorganized (23–25). Microvasculature in rat gliomas is 2–3 times as large as that within normal cortex, and vessels may be as large as 250 μm (24, 25). These dimensions are well within the range of the 8-T imaging. Therefore, it should be possible to identify areas of increased microvascularity in brain tumors at 8-T imaging (18).

In this study, the MR imaging findings of distorted vasculature in the tumor included enlargement of transmedullary veins, increased tortuosity, and generally increased overall vessel density. Other investigators have demonstrated that apparent vessel density in a nude mouse glioma model, as identified on 4.7-T GE MR images, correlates with the histopathologically identified density of blood-containing vessels (8) and can be used to quantify angiogenesis in this same animal model (9, 10). In these studies, vascular density was quantified from signal intensity loss on susceptibility-weighted images due to the paramagnetic property of deoxyhemoglobin (8–10, 26). Correlation to histopathologically determined vessel density measured immediately post mortem was statistically significant ($P = .0001$, $n = 35$, $r = 0.905$) (9, 26). The inhomogeneity of the signal intensity received from the acquired images may also lead to underestimation or overestimation of angiogenic contrast. We believe this AVD determination helps to supplement the direct visualization of tumoral microvasculature and is presumed to be representative of the MVD in the sampled region beyond the resolution of 8-T imaging. Because field inhomogeneities encountered with 8-T MR imaging may lead to large variations in the AVD calculations, these calculations must be validated in a large patient population. Reduction of field inhomogeneity should help reduce this problem.

Other groups have demonstrated high-resolution imaging of the venous structures of the brain by using blood oxygenation level–dependent GE imaging similar to our techniques in that they both rely on longer TE GE imaging (27–31). The advantage of imaging at the higher magnetic field of 8 T is that the signal-to-noise ratio is substantially higher; therefore, the resolution is higher. The 8-T images can be acquired at a substantially shorter TE because the T2* of deoxyhemoglobin in the veins is short.

Although our results are not conclusive, they demonstrate good agreement between areas of increased vascularity at 8-T imaging and histopathologic analysis. Image analysis based on signal intensity may be confounded only in regions of necrosis, hemorrhage, and calcification. It is possible to differentiate these regions from foci of increased vascularity on the basis of adjacent vascular structures, morphology, and appearance of the surrounding tissues. In general, low signal intensity due to vascular structures have a serpiginous shape, and these signal voids can be followed toward the parent vessels.

Conclusion

The current study provides pilot data suggesting that direct visualization of increased microvascularity in a GBM may be possible at 8 T. These findings should be confirmed on a more consistent basis in a larger population of patients.

Acknowledgment

We wish to acknowledge Dr Pierre-Marie Robitaille, whose persevering efforts allowed for the development and function of 8-T MR imaging.

References

1. Kleihues P, Burger PC, Plate KH, Ohgaki H, Cavanee WK. **Glioblastoma.** In: Kleihues P, Cavenee WK, eds. *Pathology and genetics of tumours of the nervous system.* Lyon, France: International Agency for Research on Cancer; 1997:22
2. Brem S, Cotran R, Folkman J Tumor angiogenesis: **A quantitative method for histologic grading.** *J Nat Cancer Inst* 1972;48: 347–356
3. Robitaille PM, Warner R, Jagadeesh J. **Design and assembly of an 8 Tesla whole body MRI scanner.** *J Comp Assist Tomogr* 1999;23: 808–820
4. Weidner N. **Tumoral vascularity as a prognostic factor in cancer patients: the evidence continues to grow.** *J Pathol* 1998;184:119–122
5. Fox SB. **Tumour angiogenesis and prognosis.** *Histopathology* 1997; 30:294–301
6. Eberhard A, Kahlert S, Goede V, Hemmerlein B, Plate KH, Augustin HG. **Heterogeneity of angiogenesis and blood vessel maturation in human tumors: implications for antiangiogenic tumor therapies.** *Cancer Res* 2000;60:1388–1393
7. Vaughan JT, Hetherington HP, Out JO, Pan JW, Pohost GM. **High frequency volume coils for clinical NMR imaging and spectroscopy.** *Magn Reson Med* 1994;32:206–218
8. Abramovich R, Frenkiel D, Neeman M. **Analysis of subcutaneous angiogenesis by gradient echo magnetic resonance imaging.** *Magn Reson Med* 1998;39:813–824
9. Abramovich R, Marikovsky M, Meir G, Neeman M. **Stimulation of tumour angiogenesis by proximal wound: spatial and temporal analysis by MRI.** *Br J Cancer* 1998;77:440–447
10. Abramovich R, Meir G, Neeman M. **Neovascularization induced growth of implanted C6 glioma multicellular spheroids: magnetic resonance microimaging.** *Cancer Res* 1995;55:1956–1962
11. Burgess RE, Yu Y, Christoforidis GA. **Human Leptomeningeal and cortical vascular anatomy of the cerebral cortex at 8 Tesla.** *J Comp Assist Tomogr* 1999;23:850–856
12. Abduljalil AM, Kangarlu A, Yu Y, Robitaille PML. **Macroscopic susceptibility in ultra high field MRI, II: acquisition of spin echo images from the human head.** *J Comput Assist Tomogr* 1999;23: 842–844
13. Chen CN, Sank VJ, Cohen SM, Hoult DI. **The field dependence of NMR imaging, I: Laboratory assessment of signal-to-noise ratio and power deposition.** *Magn Reson Med* 1986;3:722–729
14. Collins CM, Smith MB. **Signal-to-noise ratio and absorbed power as functions of main magnetic field strength, and definition of "90 degrees " RF pulse for the head in the birdcage coil.** *Magn Reson Med* 2001;45:684–691
15. Cremillieux Y, Ding S, Dunn JF. **High-resolution in vivo measurements of transverse relaxation times in rats at 7 Tesla.** *Magn Reson Med* 1998;39:285–290
16. Hoult DI, Phil D. **Sensitivity and power deposition in a high-field imaging experiment,** *J Magn Reson Imaging* 2000;12:46–67
17. Vaughan JT, Garwood M, Collins CM. **7T vs. 4T: RF power, homogeneity, and signal-to-noise comparison in head images.** *Magn Reson Med* 2001;46:24–30.
18. Christoforidis GA, Grecula JC, Newton HB. **Visualization of microvascularity within glioblastoma multiforme utilizing 8 Tesla high-resolution magnetic resonance imaging.** *Am J Neuroradiol* 2002;23:1553–1556
19. Abduljalil AM, Robitaille PML. **Macroscopic susceptibility In ultra high field MRI.** *J Comput Assist Tomogr* 1999;23:832–841
20. Christoforidis GA, Bourekas EC, Baujan M. **High resolution MRI of the deep brain vascular anatomy at 8 Tesla: susceptibility-based enhancement of the venous structures.** *J Comput Assist Tomogr* 1999;23:857–866
21. Burger PC, Vogel FS, Green SB, Strike TA. **Glioblastoma multiforme and anaplastic astrocytomas: pathologic criteria and prognostic implications.** *Cancer* 1985;56:1106–1111
22. Daumas-Duport C, Scheihauer B, O'Fallon J, Kelly P. **Grading of astrocytomas: a simple and reproducible method.** *Cancer* 1988;62: 2152–2165
23. Deane BR, Lantos PL. **The vasculature of experimental brain tumours, I: A sequential light and electron microscope study of angiogenesis**. *J Neurol Sci* 1981;49:55–66
24. Zama A, Tamura M, Inoue H. **Three-dimensional observations on microvascular growth in rat glioma using a vascular casting method.** *J Cancer Res Clin Oncol* 1991;117:396–402
25. Dewhirst MW, Tso CY, Oliver R, Gustafson CS, Secomb TW, Gross JF. **Morphologic and hemodynamic comparison of tumor and healing normal tissue microvasculature.** *Intl J Radiat Oncol Biol Phys* 1989;17:91–99
26. Neeman M. **Preclinical MRI experience in imaging angiogenesis.** *Cancer Met Rev* 2000;19:39–43
27. Boxerman JL, Hamberg LM, Rosen BR, Weisskoff RM. **MR contrast due to intravascular magnetic susceptibility pertubations.** *Magn Res Med* 1995;35:555–566
28. Essig M, Reichenbach JR, Schad LR, Schoenberg SO, Debus J, Kaiser WA. **High-resolution MR venography of cerebral arteriovenous malformations.** *Magn Reson Imaging* 1999;17:1417–1425
29. Reichenbach JR, Essig M, Haacke EM. **High-resolution venography of the brain using magnetic resonance imaging.** *MAGMA* 1998:6:62–69
30. Reichenbach JR, Barth M, Haacke EM, Klarhofer M, Kaiser WA, Moser E. **High-resolution MR venography at 3.0 Tesla.** *J Comput Assist Tomogr* 2000;24:949–957
31. Reichenbach JR, Jonetz-Mentzel L, Fitzek C. **High-resolution blood oxygen-level dependent MR venography (HRBV): a new technique.** *Neuroradiology* 2001;43:364–369